BIOCHEMISTRY
including biophysical chemistry & molecular biology

Article

pubs.acs.org/biochemistry

Structure and Catalytic Mechanism of N^5,N^{10}-Methenyltetrahydromethanopterin Cyclohydrolase

Vikrant Upadhyay,[†] Ulrike Demmer,[†] Eberhard Warkentin,[†] Johanna Moll,[‡] Seigo Shima,*[,‡,§] and Ulrich Ermler*[,†]

[†]Max-Planck-Institut für Biophysik, Max-von-Laue-Straße 3, D-60438 Frankfurt am Main, Germany

[‡]Max-Planck-Institut für Terrestrische Mikrobiologie, Karl-von-Frisch-Straße, D-35043 Marburg, Germany

[§]PRESTO, Japan Science and Technology Agency (JST), Honcho, Kawaguchi, Saitama 332-0012, Japan

Supporting Information

ABSTRACT: Methenyltetrahydromethanopterin (methenyl-H_4MPT$^+$) cyclohydrolase (Mch) catalyzes the interconversion of methenyl-H_4MPT$^+$ and formyl-H_4MPT in the one-carbon energy metabolism of methanogenic, methanotrophic, and sulfate-reducing archaea and of methylotrophic bacteria. To understand the catalytic mechanism of this reaction, we kinetically characterized site-specific variants of Mch from *Archaeoglobus fulgidus* (aMch) and determined the X-ray structures of the substrate-free aMch(E186Q), the aMch:H_4MPT complex, and the aMch(E186Q):formyl-H_4MPT complex. (Formyl-)H_4MPT is embedded inside a largely preformed, interdomain pocket of the homotrimeric enzyme with the pterin and benzyl rings being oriented nearly perpendicular to each other. The active site is primarily built up by the segment 93:95, Arg183 and Glu186 that either interact with the catalytic water attacking methenyl-H_4MPT$^+$ or with the formyl oxygen of formyl-H_4MPT. The catalytic function of the strictly conserved Arg183 and Glu186 was substantiated by the low enzymatic activities of the E186A, E186D, E186N, E186Q, R183A, R183Q, R183E, R183K, and R183E-E186Q variants. Glu186 most likely acts as a general base. Arg183 decisively influences the pK_a value of Glu186 and the proposed catalytic water mainly by its positive charge. In addition, Glu186 appears to be also responsible for product specificity by donating a proton to the directly neighbored N^{10} tertiary amine of H_4MPT. Thus, N^{10} becomes a better leaving group than N^5 which implies the generation of N^5-formyl-H_4MPT. For comparison, methenyltetrahydrofolate (H_4F) cyclohydrolase produces N^{10}-formyl-H_4F in an analogous reaction. An enzymatic mechanism of Mch is postulated and compared with that of other cyclohydrolases.

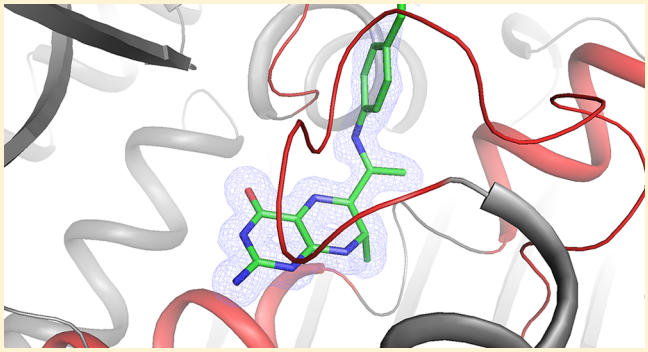

Methenyltetrahydromethanopterin (methenyl-H_4MPT$^+$) cyclohydrolase (Mch) catalyzes the reversible conversion between N^5,N^{10}-methenyl-H_4MPT$^+$ and N^5-formyl-H_4MPT (Figure 1) in the energy metabolism of various microorganisms.[1,2]

$$N^5,N^{10}\text{-methenyl-}H_4\text{MPT}^+ + H_2O \rightleftharpoons N^5\text{-formyl-}H_4\text{MPT} + H^+ \quad \Delta G^{\circ\prime} = +5\ \text{kJ/mol}$$

In methanogenic archaea,[3] methane is formed from a few one-carbon compounds like CO_2, methanol, and methylamine requiring the cyclohydrolase reaction in the backward direction. Sulfate-reducing archaea[4] and methylotrophic bacteria[5] use this reaction only in the forward direction by metabolizing lactate and methanol, respectively, to CO_2.[4−6] In addition, recent genomic studies indicated that methanotrophic archaea use Mch in the one-carbon metabolism from methane.[7]

Mch has been purified and characterized from various organisms including *Methanobacterium thermoautotrophicum*,[8] *Methanothermobacter marburgensis*,[9] *Methanosarcina barkeri*,[10] *Methanopyrus kandleri*,[11] *Archaeoglobus fulgidus*,[4] and *Methanobacterium extorquens* AM1.[12] Some of these enzymes have been heterologically overproduced.[12,13] Mch has a molecular mass of around 35 kDa and hosts no prosthetic group.[4,12,13] In the crystal structure of Mch from the hyperthermophilic methanogenic archaeon *M. kandleri*, the enzyme is present in a homotrimeric state.[14] The sequence identity between Mch from different organisms with known primary structures is beyond 40%.

A reaction analogous to Mch is performed by methenyltetrahydrofolate (methenyl-H_4F$^+$) cyclohydrolase[15,16] (N^5,N^{10}-methenyl-H_4F$^+$ + H_2O ⇌ N^{10}-formyl-H_4F + H^+, $\Delta G^{\circ\prime}$ = −6 kJ/mol), which operates with H_4F as a one-carbon carrier. H_4F, found in all organisms, is structurally and functionally analogous to H_4MPT (Figure 1) and plays a central role in

Received: June 12, 2012
Revised: September 21, 2012
Published: September 26, 2012

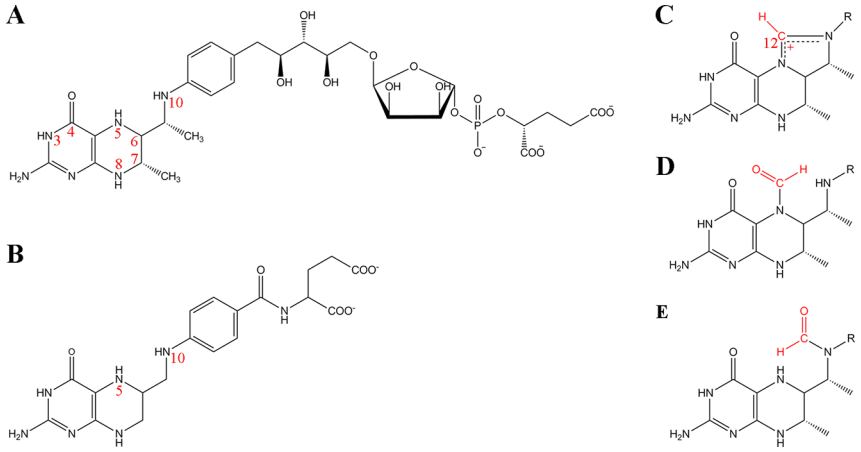

Figure 1. Structures of (A) H_4MPT, (B) H_4F, (C) N^5,N^{10}-methenyl-H_4MPT$^+$, (D) N^5-formyl-H_4MPT, and (E) N^{10}-formyl-H_4MPT.

the amino acid and nucleic acid metabolism. Methenyl-H_4F^+ cyclohydrolase (34 kDa) occurs either as a bifunctional enzyme with an additional methylene-H_4F dehydrogenase activity or as a trifunctional enzyme containing a further domain with a H_4F synthetase activity (67 kDa).[17] The crystal structure of methenyl-H_4F^+ cyclohydrolase has been solved from several organisms[17−19] [PDB codes 2C2X and 3L07]. Structural data about its complex with formyl-H_4F or methenyl-H_4F^+ have not been reported so far. A catalytic mechanism has been proposed for the human enzyme based on structures of enzyme-folate analogue complexes,[20] kinetic data from site-specific enzyme variants,[21] and chemical properties of methenyl-H_4F^+ investigated 40 years ago in solution.[22−24] Hydrolysis/formation of cyclic formamidinium ions, in particular, methenyl-H_4F^+ was mechanistically divided into a nucleophilic addition of OH^- to the formamidinium ion and into a decomposition of the tetrahedral addition intermediate. The latter was spectroscopically detectable in solution under strong alkaline conditions.[25] The product-determining ring cleavage step proceeds either by a general acid (pH < 3) or a general base mechanism (pH > 3) catalyzing the breakdown of an anionic or cationic intermediate, respectively.

Coenzymes H_4MPT and H_4F primarily differ in the p-aryl substituent (Figure 1). While the methylene substituent in H_4MPT donates electrons to the aromatic ring, the carbonyl group of H_4F withdraws electrons. This property is reflected in a pK_a of 2.4 and −1.2 for N^{10} of H_4MPT and H_4F,[26,27] respectively, and lower redox potentials for H_4MPT derivatives. Although H_4MPT and H_4F dependent enzymes catalyze analogous reactions, the involved enzymes and the enzymes catalyzing the biosynthesis of H_4MPT and H_4F are structurally different, indicating an independent development of the two one-carbon carriers during evolution.[28]

As structure analysis of an enzyme−substrate complex failed with the *M. kandleri* Mch,[14] we choose as alternative target the *Archaeoglobus fulgidus* Mch, termed as aMch. In the anaerobic hyperthermophilic sulfate-reducing archaeon *A. fulgidus*, lactate is oxidized to acetyl-CoA via pyruvate and further to CO_2 via the H_4MPT and methanofuran dependent C_1 pathway.[29,30] One reaction of the C_1 pathway is catalyzed by aMch which has an optimum activity at 85 °C and at a pH of 8.5. The Michealis-Menton kinetics yielded a K_m value of 220 μM for methenyl-H_4MPT$^+$ and a specific activity of 1770 U/mg.[4] Interestingly, the kinetic behavior between aMch and Mch from *M. kandleri* differs with respect to the effect of lyotropic salts (e.g., K_2HPO_4) on the activity and the stability. aMch requires K_2HPO_4 (1 M) for stabilization at 90 °C but not for the activity, whereas Mch from *M. kandleri* requires K_2HPO_4 (1.5 M) for activity but not for thermostability.[4] In this report, we describe the kinetic characterization of several aMch variants with site-specific exchanged amino acids in the active site and the crystal structure of aMch (E186Q) in an empty state and of aMch (wild type) and aMch (E186Q) in complex with H_4MPT and formyl-H_4MPT, respectively. On the basis of these data, a catalytic mechanism for the Mch reaction is postulated.

EXPERIMENTAL PROCEDURES

Cloning of the aMch Gene. The *mch* open reading frame of the genomic DNA from *A. fulgidus* was amplified by PCR. Primers for PCR amplification are listed in Table S1 in the Supporting Information. The 50 μL PCR reaction contained 200 μM d-NTP, 0.2 μM of each primer, 500 ng of genomic DNA of *A. fulgidus* as a template, and 1.0 U Phusion DNA polymerase (Finnzymes). The temperature program was 30 s at 98 °C, 30 cycles 10 s at 98 °C/10 s at 50.4 °C/30 s at 72 °C and 7 min at 72 °C. The PCR product was purified and cloned into the pDrive vector using the PCR purification and cloning kits of Qiagen, respectively, according to the protocol of the manufacturer. *E. coli* DH5α cells were transformed with pDrive-Mch plasmid, and positive clones were selected by standard blue/white screening. After DNA sequencing for control, the pDrive-Mch plasmid was cleaved with *Eco*RI and *Nde*I restriction enzymes and ligated into the expression vector pET-24a(+).

Preparation of Mutants. Mutagenesis of the *mch* gene from *A. fulgidus* was conducted by the QuikChange site-directed mutagenesis kit protocol (Stratagene). pET-24a(+)-*mch* was used as template for mutagenesis. Mutagenic primers are listed in Table S1 in the Supporting Information. The sequences of the desired mutant alleles were confirmed by sequencing.

Overexpression and Purification. Wild type and mutated variants of aMch were overexpressed in *E. coli* Rosetta (DE3) pLysS strain. All the steps if not specified were performed at 4 °C. Recombinant *E. coli* cells were grown aerobically at 37 °C in 1 L of Luria−Bertani medium supplemented with kanamycin (30 μg/mL) and chloramphenicol (34 μg/mL). When the absorbance at 600 nm of the culture had reached 0.6, isopropyl β-D-1-thiogalactopyranoside was added to a final concentration of 0.5 mM. Cells were harvested by an absorbance of 2.0 at 600

dx.doi.org/10.1021/bi300777k | *Biochemistry* 2012, 51, 8435−8443

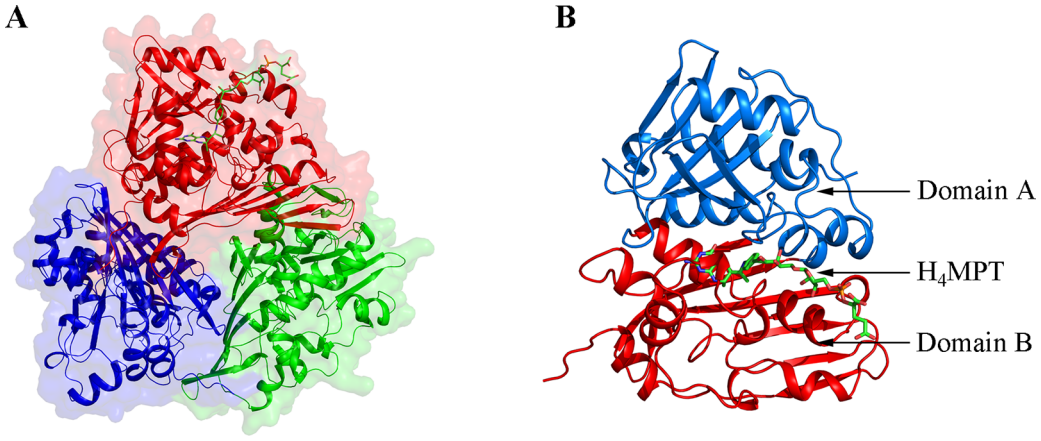

Figure 2. X-ray structure of aMch. (A) Homotrimer. The subunits are shown in red, blue, and green and the molecular surface in a transparent manner. The substrate N^5-formyl-H_4MPT painted as a stick model is bound to one subunit with a significant occupancy. (B) Monomer. The substrate binding site is located in a pocket between domains A (blue) and B (red).

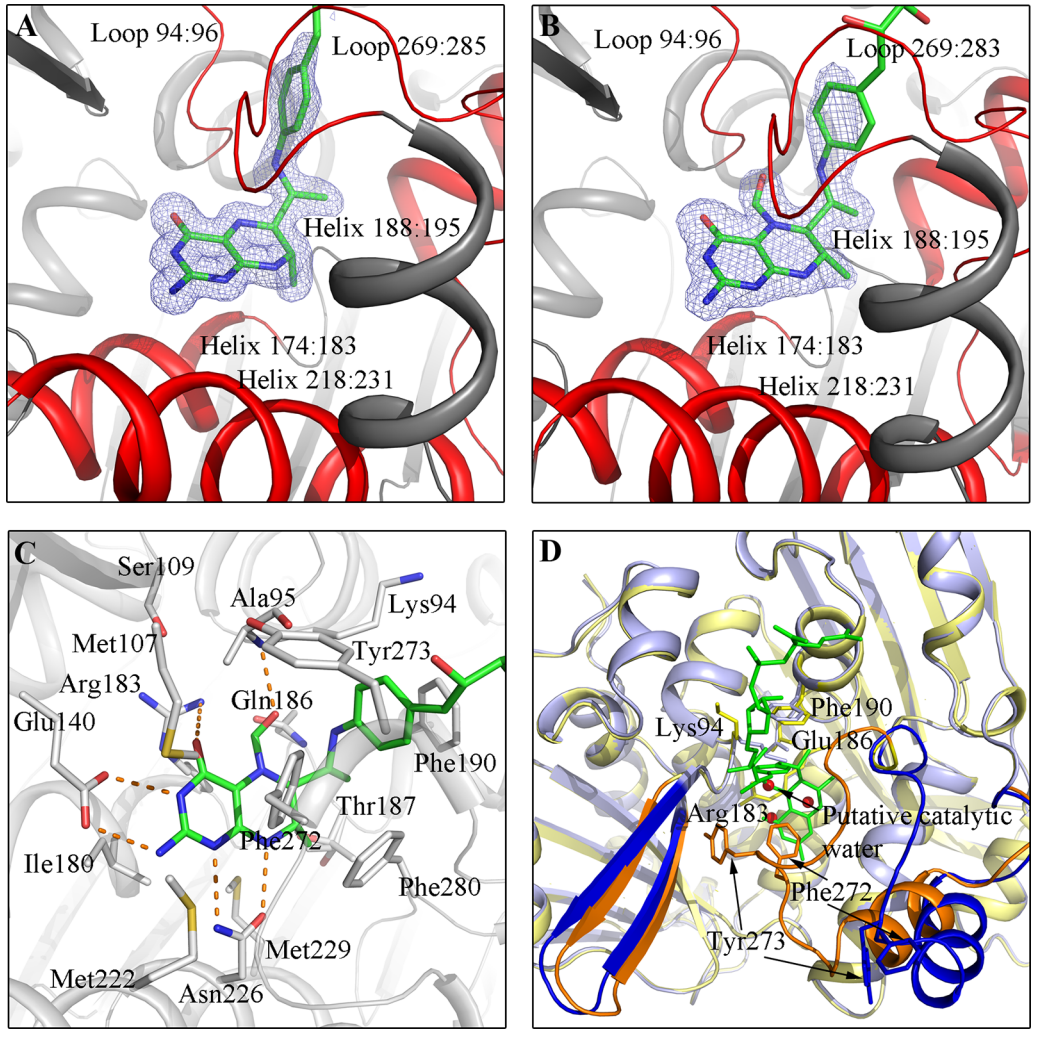

Figure 3. Substrate binding (A) H_4MPT and (B) N^5-formyl-H_4MPT. The electron density is shown in light-blue at a contour level of 1.0σ. The polypeptide is shown in a ribbon presentation (gray), and segments that interact with (formyl-)H_4MPT are highlighted in red. Notably, helices 174:183 and 188:195 can be also described as a single bent helix. (C) The interactions between the formyl-H_4MPT and the protein matrix. Residues contacting the pterin ring are drawn as sticks. Hydrogen bonds are painted as dashed lines. (D) aMch structures with (yellow) and without (light-blue) substrate superimposed. H_4MPT binding induces a conformational change of a few segments highlighted in orange and blue. In the empty aMch structure, the H_4MPT binding site is occupied by several firmly bound solvent molecules. The putative catalytic water is highlighted by an arrow.

dx.doi.org/10.1021/bi300777k | *Biochemistry* 2012, 51, 8435−8443

nm, centrifugated, and resuspended in 9 mL of 50 mM Tris/HCl pH 7.0 and 0.5 mM phenylmethylsulfonyl fluoride. Cell extract was disrupted by ultrasonification, and the cell lysate was ultracentrifugated at 4 °C for 90 min at 100 000*g* . Most proteins in the supernatant were precipitated by heat denaturation at 80 °C for 30 min in 0.5 M K_2HPO_4/HCl, pH 8.0 and removed by ultracentrifugation at 4 °C for 60 min at 100 000*g*. aMch in 50 mM Tris/HCl pH 7.0 and 1 M ammonium sulfate was loaded onto a Phenyl sepharose HP (GE Lifesciences) column and eluted with 1.0, 0.5, 0.25, and 0 M ammonium sulfate in 50 mM Tris/HCl pH 7.0. aMch was found in the fraction with 0 M ammonium sulfate fraction. aMch was further purified by size exclusion chromatography using a Superdex 200 prep grade column (GE Lifesciences) and 50 mM Tris/HCl pH 7.0 and 150 mM NaCl as elution buffer.

Kinetic Analysis. Methenyl-H_4MPT^+ was semisynthesized from a cell suspension of *M. marburgensis* as described earlier.[31] The specific activity of wild type and mutated variants of aMch was determined at 65 °C.[4] The reaction mixture (700 μL) contained 50 mM Tris/HCl pH 7.6 (at 65 °C) and 30 μM methenyl-H_4MPT^+. The reaction was started by adding enzyme solution diluted in 50 mM Tris/HCl, pH 7.6 at 65 °C to a final concentration of ~3 μg/mL. Concentration of methenyl-H_4MPT^+ was varied in reaction mixtures for determining the K_m and V_{max} values. The hydrolysis of methenyl-H_4MPT^+ was followed by the absorption decrease at 336 nm (ε_{336} = 21.6 mM^{-1} cm^{-1}). Values for K_m and V_{max} were determined from the Michaelis–Menten equation[32] using the program SigmaPlot 12 for nonlinearized curve fitting. Protein was quantified by the Bio-Rad protein assay (Bio-Rad Laboratories GmbH) with a bovine serum albumin standard.

Crystallization. Before crystallization, aMch was concentrated to ~40 mg/mL and stored in 10 mM MES/NaOH, pH 5.5. Crystallization experiments with the enzyme (15 mg/mL) supplemented with methenyl-H_4MPT^+ were performed by the hanging drop vapor diffusion method in an anaerobic tent with an atmosphere of 95% N_2/5% H_2 under low-intensity red light because of the O_2 and light sensitivity of H_4MPT. The JBS Classic Kit (Jena Bioscience) was used for screening. The detailed crystallization conditions are listed in Table 2.

Structural Determination. Data for empty aMch(E186Q) and for aMch and aMch(E186Q) both soaked with methenyl-H_4MPT^+ were collected at the SLS-PXII beamline in Villigen, Switzerland, at resolutions of 1.5, 1.3, and 1.75 Å, respectively. After indexing, integrating, and scaling the data using the program XDS,[33] the structure was determined by the molecular replacement method using the program PHASER[34] and the coordinates of Mch from *M. kandleri*[14] as the initial search model. Iterative cycles of refinement and manual building were performed with programs REFMAC5[35] and COOT,[36] respectively. The initial cycles of refinements were carried out without methenyl-H_4MPT^+ and water molecules, which were afterward incorporated if the $2F_o - F_c$ and $F_o - F_c$ electron densities were beyond a contour level 1 and 3σ, respectively. Maximum likelihood minimization with (an)isotropic *B*-value refinement and several modifications in the geometry file of the substrate lead to the final results. Structural interpretations were based on normalized $2F_o - F_c$ and $F_o - F_c$, and the corresponding omit electron density maps. The quality of the models was checked by the program PROCHECK.[37] Figures 2, 3, and 4 were produced by PYMOL.[38]

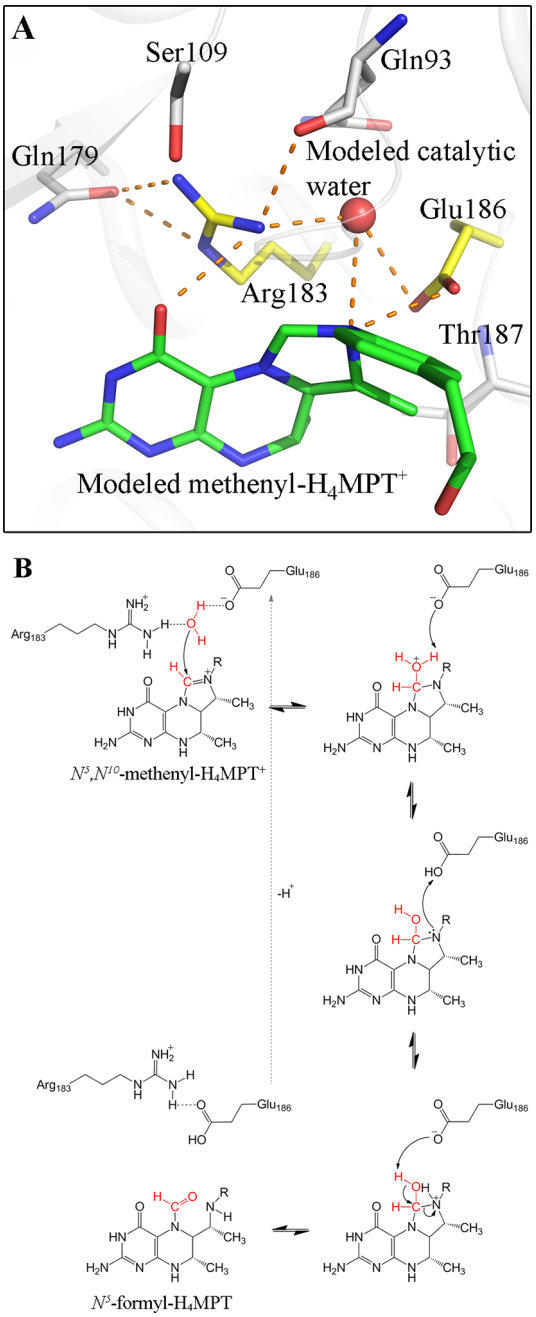

Figure 4. The aMch reaction. (A) Active site architecture. Methenyl-H_4MPT^+ and the catalytic water (red) were modeled as described in the text. The N^5 and N^{10} atoms of methenyl-H_4MPT^+ (C atoms in green) interact with Arg183 and Glu186 (C atoms in yellow), respectively, and the C^{14} atom is in van der Waals contact to Ala95, Arg183, and Phe272. Hydrogen bonds are painted as dashed lines. (B) Mechanism. The enzymatic mechanism of the reversible Mch reaction consists of a nucleophilic addition of an activated water molecule and a ring-cleavage elimination step. The structural data suggest that Arg183 and Glu186 are directly hydrogen-bonded in the aMch-(E186Q):formyl-H_4MPT structure and via the catalytic water in the aMch:methenyl-H_4MPT^+ structure.

RESULTS AND DISCUSSION

Production and Kinetic Analysis of Native and Site-Directed Mutated aMch. aMch was heterologously produced and isolated in a pure and homogeneous form with a yield of around 10 mg from 1 L of culture. To explore the function of

dx.doi.org/10.1021/bi300777k | *Biochemistry* 2012, 51, 8435–8443

catalytically relevant active site residues, site-directed mutagenesis experiments were performed, and the corresponding Mch variants were purified as described for the wild type. Targets for mutagenesis were chosen on the basis of the crystal structure of the *M. kandleri* Mch and of the aMch:H_4MPT complex (already available in an early stage of the project and described below). In particular, Lys94, Arg183, and Glu186 were considered as attractive candidates. While Arg183 and Glu186 are strictly conserved, Lys94 is only moderately conserved (Figure S1 of the Supporting Information) and its side chain appears to point away from the active site. In addition, we created the F190V mutant, because the benzyl groups of Phe190 and H_4MPT seem to contact each other. The Mch reaction obeys Michaelis–Menten kinetics; values of V_{max} and K_m of the aMch variants are listed in Table 1.

Table 1. Kinetic Properties of Active Site Mutants of aMch

enzyme	V_{max} (U/mg)	K_m (μM)
wild type	10000 ± 1400	55 ± 13
E186A	3.5 ± 0.3	26 ± 5
E186D	56 ± 5	62 ± 9
E186N	10 ± 1	50 ± 11
E186Q	N.D.[a]	N.D.[a]
R183A	7.0 ± 0.4	43± 5
R183Q	5.1 ± 0.8	43 ± 11
R183E	1.2 ± 0.1	25 ± 4
R183K	1500 ± 40	43 ± 2
R183E-E186Q	N.D.[a]	N.D.[a]
K94V	4100 ± 400	47 ± 9
K94E	8600 ± 1100	77 ± 15
F190V	N.D.[a]	N.D.[a]

[a]Not detectable.

Glu186 was mutated to glutamine, aspartate, asparagine, and alanine. Its essential function was reflected in the drastically reduced enzymatic activities ranging from a factor of ~180 for the E186D variant to nearly inactive for the E186Q variant. Arg183, site-specifically exchanged to alanine, glutamate, glutamine, and lysine, crucially affect catalysis. In particular, the positive charge turned out to be an important factor. The variants K94V and K94E exhibited strongly reduced but still significant activity and thus indicate that Lys94 is not directly involved in catalysis as suggested by the aMch:H_4MPT structure. The branched valine side chain might slightly displace H_4MPT and thus cause the reduced enzymatic activity. The F190V exchange resulted in a very low activity reflecting its crucial function in binding/adjusting the benzyl ring of H_4MPT. The K_m values of the produced enzyme variants, ranging from 25 to 77 μM, are not substantially influenced by the amino acid exchanges.

Structural Basis. Crystallization of aMch readily succeeded under aerobic conditions, and the data set with the highest resolution was collected with the Mch(E186Q) variant. Its structure was determined with the molecular replacement method using *M. kandleri* Mch as a search model (Table 2). aMch was found as a homotrimer (105 kDa); each monomer can be architecturally subdivided into the two closely associated domains A (1-57, 83-170) and B (58-82, 171-316) (Figure 2). Both of them adopt an α/β structure with a six-stranded mixed β-sheet, however, with different strand topologies and α-helix positions.[14] The root-mean-square (rms) deviation between aMch and Mch of *M. kandleri* monomers is 0.45 Å (98% of the C_α used); their sequence identity is 53%. Structural deviations only include the N- and C-terminal ends, the loop following strands 62:64 and 233:239, and the expanded linker between helix 244:248 and strand 284:289 (Figure S2 of the Supporting Information). The conformational differences of the latter segment are, however, primarily due to the absence/presence of the substrate in the active site (see below). According to the DALI server,[39] the Mch monomer adopts a unique fold not found in any protein of the protein data bank.[40] This also holds true for the individual domains.

Table 2. Data Collection and Refinement Statistics

data set	aMch(E186Q)	aMch + H_4MPT	aMch(E186Q) + N^5-formyl-H_4MPT
cystallization conditions	10% (w/v) PEG 4000	14% (w/v) PEG 4000	8% (w/v) PEG 4000
	10% (v/v) isopropanol	0.4 M ammonium acetate	0.1 M ammonium acetate
	0.1 M sodium acetate pH 5.6	0.1 M sodium acetate pH 4.6	0.1 M sodium acetate pH 4.6
	10 mM MES, pH 5.5, 0.1 M NaCl	10 mM MES, pH 5.5, 0.1 M NaCl	10 mM MES, pH 5.5, 0.1 M NaCl
		5 mM N^5, N^{10}-methenyl-H_4MPT$^+$	5 mM N^5, N^{10}-methenyl-H_4MPT$^+$
Data Collection			
wavelength (Å)	1.0001	0.979	1.214
space group	*C*2	$P2_12_12_1$	$P2_12_12_1$
unit cell parameters *a*, *b*, *c* (Å)	118.5, 122.1, 79.4	92.6, 94.2, 114.9	91.9, 109.0, 114.9
β (deg)	99.0		
no. of trimers in the asymmetric unit	1	1	1
resolution range (Å) (highest shell)	50–1.2 (1.77–1.52)	50–1.3 (1.35–1.3)	50.0–1.75 (1.85–1.75)
redundancy	5.7 (5.4)	4.8 (2.4)	4.0 (2.7)
completeness (%)	96.3 (91.0)	93.8 (69.3)	92.8 (75.8)
R_{sym} (%)	6.6 (30.2)	5.4 (31.3)	8.5 (37.5)
$I/\sigma(I)$	15.2 (4.6)	18.7 (3.5)	14.7 (3.1)
Refinement			
resolution limit (Å)	50.0–1.5	50.00–1.3	50.0–1.75
R_{work}/R_{free}	16.4/23.1	13.4/16.1	18.7/24.4
no. of residues	945	945	945
no. of solvent molecules	740	953	510
rmsd bond lengths (Å)	0.0184	0.011	0.019
rmsd bond angles (deg)	1.9	1.54	2.0
average *B* (Å^2) protein, substrate, solvent	23.7, –, 38.3	15.0, 22.3, 31.8	28.3, 32.2, 37.6

aMch and methenyl-H_4MPT$^+$ were cocrystallized under red light and strictly anaerobic conditions, which results in a structure of the aMch:H_4MPT complex at 1.3 Å resolution and the aMch(E186Q):formyl-H_4MPT complex at 1.75 Å resolution (Table 2). In the crystallization drops, methenyl-H_4MPT$^+$ was converted to formyl-H_4MPT even though the reaction thermodynamically favors methenyl-H_4MPT$^+$ formation at the used pH of 5.5. H_4MPT could be formed by hydrolysis of the formyl group from formyl-H_4MPT. Multiple cocrystallization and soaking experiments to establish the aMch:methenyl-H_4MPT$^+$ structure failed even when the nearly inactive E186Q variant was applied. Perhaps, the enzyme in the crystalline state is fixed in a conformation in which the ring-forming reaction cannot be catalyzed and thus formyl-H_4MPT

dx.doi.org/10.1021/bi300777k | *Biochemistry* 2012, 51, 8435–8443

accumulates over time. Although the adjacent subunits of the homotrimer are far away from the substrate binding site (Figure 2A) and do not specifically affect substrate binding, the occupancy of formyl-H_4MPT and H_4MPT varies between the three monomers of the asymmetric unit. Structure description is therefore related to the monomers with the best occupied ligands.

Binding of H_4MPT and Formyl-H_4MPT. The substrate binding site is localized in a deep pocket between domains A and B (Figure 2B) as already predicted on the basis of a profile and conservation analysis of the protein surface of *M. kandleri* Mch.[14] In the aMch:H_4MPT and aMch(E186Q):formyl-H_4MPT structures, the ligands are clearly visible in the electron density; their occupancy was estimated to be ∼70% (Figure 3A,B). The pterin ring is embedded into the interdomain pocket with its entire *si*-face attached to the bottom. The benzyl ring is nearly perpendicularly oriented to the pterin ring and flanked (together with the ribitol) by the wall of the pocket (Figure 3). The flexibility continuously increases from the pterin ring to the benzyl group reflected in *B* factors of ∼30 Å^2 for the pyrimidine ring, ∼40 Å^2 for the tetrahydropyrazine ring, and nearly 60 Å^2 for the benzyl ring. The residual parts of H_4MPT are solvent-exposed and completely disordered. The bottom of the pocket is formed by helix 174:183 and its wall by helix 188:195, helix 218:231, the expanded linker between helix 244:248 and strand 284:289, as well as the flat side of the central β-sheet of domain A (Figure 3A,B). Notably, the chain following the short strand 96:101 of the central β-sheet turned at Ala95 toward the substrate binding site and then continued by helix 85:93, parallel to strand 96:101.

Because of the space requirement of the formyl group, H_4MPT and formyl-H_4MPT slightly differ in their position and conformation. To evade steric hindrance between the formyl group and the protein matrix, the pterins of formyl-H_4MPT and H_4MPT are mutually shifted by ∼0.3 Å parallel to the pocket bottom. Atoms C^6 and C^7 of the tetrahydropyrazine rings deviate differently from planarity. As a consequence, the C^7 methyl group points to the *re*-face in H_4MPT but approximately sits in the pterin plane in formyl-H_4MPT. Interestingly, the distance between atoms N^5 and N^{10} is ∼0.5 Å longer in formyl-H_4MPT than in H_4MPT. Therefore only in the latter, atoms N^5, N^{10}, and C^{11} are in a relative position that directly allows the modeling of the imidazolidine ring (Figure 3A,B).

(Formyl)-H_4MPT is multiply connected to the polypeptide chain (Figure 3C). The pterin ring is sandwiched between Met107, Met222, Phe272, and Phe280 pointing to its *si*-face and Ile180, Arg183, Thr187, and Met229 pointing to its *re*-face. Hydrogen bonds are formed between the amine *N* and N^3 atoms of the pyrimidine ring and Glu140-$O_{\varepsilon 1}$ and -$O_{\varepsilon 2}$, between atom N^1 and Asn226-$N_{\delta 2}$ and between atom O^4 and several solvent molecules linked to Tyr52, Ser109, and Arg183. The N^8 atom of the tetrahydropyrazine ring is hydrogen-bonded with the Asn226-$O_{\delta 1}$. Its N^5 atom is hydrogen-bonded with Arg183 in the aMch:H_4MPT, while in the aMch-(E186Q):formyl-H_4MPT structure their distance of 3.8 Å is significantly increased due to the mentioned shift of the pterin ring. The formyl oxygen is hydrogen-bonded with Ala95-NH and Glu186-$O_{\varepsilon 1}$ (Figure 3C). No larger conformational changes are found between Glu186 in the wild type aMch and Gln186 in the aMch (E186Q) variant and between their environments. The benzyl group of (formyl-)H_4MPT is enveloped by Lys94, Phe190, Phe272, and Tyr273. Its electron density is already smeared, but its position is unambiguous and corroborated by the inactivity of the F190V variant.

Interestingly, a comparison between the aMch (E186Q) and aMch(E186Q):formyl-H_4MPT/aMch:H_4MPT structures indicates an induced-fit movement of the conformationally variable segment 254:280 (up to 7 Å for Tyr273; the distance depends on the considered monomer of the asymmetric unit), and Phe190 (0.7 Å) toward the benzyl group which decreases the pocket and optimizes the contacts to the substrate (Figure 3D). Lys94 partly occupies the benzyl binding site of H_4MPT in aMch(E186Q) but is turned toward Tyr122 in the substrate bound enzyme structures (Figure 3C,D). Interestingly, the mentioned residues moving upon H_4MPT binding are largely found in one conformation corroborating our interpretation that (formyl)-H_4MPT becomes increasingly flexible and not partially cleaved after the pterin ring.

Methenyl-H_4MPT$^+$ Modeling and Active Site Architecture. The active site of aMch is primarily formed between atoms N^5 and N^{10} of H_4MPT and Arg183, Glu186, and the backbone of the loop segment 93:95. The carboxylate group of Glu186 is surrounded by hydrophobic atoms of Lys94, Arg183, Phe190, and H_4MPT and the guanidino group of Arg183. Arg183 is strongly fixed in its position by interactions with Gln93, Ser109, Gln179, and Glu186 (Figure 4A). When comparing the three structures determined, the carboxylate group of Glu186 is conformationally rather mobile, whereas the guanidino groups of Arg183 is accurately fixed in the same position. Model building of methenyl-H_4MPT$^+$ was guided by the observed positions of the pterin and benzyl rings in the aMch:H_4MPT structure considered as anchor points and by methenyl-H_4MPT$^+$ in the conformation found in the formaldehyde-activating enzyme where the angle between the pterin and the benzyl rings is also nearly 90°.[41] Both specifications allow a fairly accurate definition of the binding mode of the imidazolidine ring and its interactions with the polypeptide (Figure 4A). Between Ala95, Arg183, and Glu186 is space for one solvent molecule termed as the catalytic water. It is visible in the electron density of the aMch(E186Q) structure (Figure 3D) and sits adjacent to the formyl oxygen of formyl-H_4MPT of a superimposed aMch(E186Q):formyl-H_4MPT structure. The catalytic water molecule becomes completely shielded from bulk solvent upon substrate binding (Figure 4A).

Catalytic Mechanism. On the basis of the hydrolysis reaction of methenyl-H_4F^+ in solution[22−24] and the binding mode of methenyl-H_4MPT$^+$(modeled)/formyl-H_4MPT presented above, a base-catalyzed mechanism for the aMch reaction is postulated (Figure 4B). In the first step after binding of methenyl-H_4MPT$^+$, the catalytic water attacks the C^{14} atom of the imidazolidinium ion from the *si*-face. Its nucleophilicity is increased by hydrogen bonds to Ala95, Arg183, and Glu186, the latter being able to act as a general base and to accept a proton. A tetrahedral imidazolidin-2-ol intermediate is formed and, in parallel, the protonated Glu186 donates the accepted proton to the adjacent N^{10} tertiary amine. Considering that N^5 is close to the Arg183 guanidino group and, in particular, N^{10} is in hydrogen-bond contact to the protonated Glu186, N^{10} becomes preferentially protonated compared to N^5 and thus the superior leaving group. In a second step, the ring is, consequently, cleaved between C^{14} and N^{10} forming the product N^5-formyl-H_4MPT (experimentally proven).[2,12,42] The breakdown step is again assisted by Glu186 that accepts as a general base the proton of the C^{14} hydroxyl intermediate. The pH optimum of 8.5 for methenyl-H_4MPT$^+$

hydrolysis by aMch[4,11,12] supports the proposed based-catalyzed mechanism. In the reverse reaction, Glu186 donates a proton to the generated C^{14} hydroxylate ion upon attack of the N^{10} amine, accepts a proton from the formed ammonium ion, and finally donates a proton to the eliminated hydroxyl group (Figure 4B).

The kinetic behavior of the produced aMch variants essentially substantiates the proposed mechanism. Mutations of the strictly conserved Glu186 clearly demonstrate the use of its proton donor/acceptor properties for catalysis (Table 1). The E186Q variant is nearly inactive (lower than 1 U/mg) although the hydrogen bond pattern is maintained and the pterin ring and the active site residues are in similar positions as experimentally verifiable by comparing the aMch:H_4MPT and aMch(E186Q):formyl-H_4MPT structures. Although the leaving group potential of the N^{10} amine is drastically reduced in the E186Q mutant, N^5- and not N^{10}-formyl-H_4MPT is still formed (see Figure 3B). It might be speculated that Glu186 participates in hydrolyzing the amide bond of N^5-formyl-H_4MPT to formic acid and H_4MPT, as the formyl group found in the aMch(E186Q):formyl-H_4MPT has disappeared in the aMch:H_4MPT structure determined under related conditions (Figure 3A,B). As expected, the E186D variant is catalytically more competent than other Glu186 variants that documents on one hand the importance of its acid−base property, especially in comparison to the E186N variant. On the other hand, the decrease of activity by a factor of 180 compared to the wild type enzyme demonstrates the importance of the position of the carboxylate group to build up a productive active site structure and the impossibility to adequately place an additional water molecule as a proton shuttle between Asp186 and the catalytic water or atom N^{10} due to the limited space. No activity was detectable for the R183E-E186Q variant indicating that the general base has to be in direct contact with atom N^{10}. Arg183 as important as Glu186 operates primarily by its positive charge demonstrated by the decrease of enzymatic activity by a factor of 8 in the R183K, of ∼2000 in the R183A and R183Q variants, and of ∼8000 in the R183E variant (Table 1). However, the activation of the catalytic water and Glu186 by pK_a adjustment is disturbed by the shorter side chain of lysine compared to arginine. In addition, an optimal formation of the active site framework is prevented (Figure 4A).

The methylene-H_4F dehydrogenase/cyclohydrolase reaction is also catalyzed by a general acid/base mechanism. However, in methylene-H_4F dehydrogenase/cyclohydrolase, the catalytic base is a lysine[20,21] and not a glutamate as in Mch. Both residues operate very specifically in their environment, and their site-specific exchange results in a weakly active or even inactive enzyme. Despite the different pK_a of their side chains both activate a water molecule by (partial) proton abstraction, donate directly or indirectly a proton to N^5 or N^{10}, respectively, and accept a proton from the tetrahedral imidazolidin-2-ol intermediate forming N^{10}-formyl-H_4F or N^5-formyl-H_4MPT. Although the structures of the reported methenyl-H_4F cyclohydrolase inhibitor complexes only create an approximate picture of the active site geometry,[20] it appears that the distance between the catalytic lysine and N^5 and N^{10} is similar and too long for a direct hydrogen bond. Additionally, since no other proton donor contacts N^5 or N^{10}, we assume that their basicity is only slightly influenced from their protein surrounding and primarily depends on their intrinsic pK_a values. The higher pK_a value of 4.2/4.2 for N^5 compared of 2.4/−1.2 for N^{10} in H_4MPT/H_4F implicates better proton acceptor and leaving group capabilities for N^5, which is reflected in the hydrolysis of methenyl-H_4F^+/H_4MPT^+ to N^{10}-formyl-H_4F/H_4MPT in an enzyme-free, strongly basic solution.[24] Notably, N^{10}-formyl-H_4F formed under kinetic control undergoes slow isomerization to the thermodynamically more stable N^5-formyl-H_4F in a weakly basic medium.[43] In Mch, N^5-formyl-H_4MPT is formed as the N^{10} amine is the preferred leaving group due to the microscopic pK_a increase by the neighboring Glu186 carboxylate group.

Catalysis of formamidinium hydrolysis/formation reactions in other metabolic processes are based on the same general principles of carbonyl oxygen/water and attacking/leaving amine group activation; however, the type of (Lewis) acids or bases differ. For example, the archaeal inosine-5-monophosphate cyclohydrolase reaction catalyzing the terminal pyrimidine ring closure step of purin biosynthesis use a glutamate as a general acid to protonate a hydroxyl group for facilitating ring formation, whereas in the reaction of the human enzyme, a lysine via a water molecule accomplishes this function.[44,45] For prosthetic group biosynthesis of the green fluorescence protein and substrate activation in class I aldolases (forming a Schiff-base adduct between a lysine of the enzyme and a ketose substrate), a glutamate again serves as a proton donor for the corresponding hydroxyl group.[46,47] In contrast, GTP cyclohydrolases I, II, and III involved in the biosynthesis of several cofactors activate water for an attack of the imidazol ring of GTP by Zn^{2+} or Mg^{2+}.[48−50]

■ ASSOCIATED CONTENT

Ⓢ Supporting Information

Table S1, list of primers used for amplification of mch gene from *A. fulgidus* and for mutagenesis; Figure S1, Mch sequences aligned; and Figure S2, aMch and Mch of *M. kandleri* superimposed. This material is available free of charge via the Internet at http://pubs.acs.org.

Accession Codes

The atomic coordinates and the crystallographic structure factors of the aMch(E186Q), aMch:H_4MPT and aMch-(E186Q):formyl-H_4MPT structures were deposited at the RCSD Protein Data Bank under the PDB accession codes 4GVR, 4GVQ and 4GVS.

■ AUTHOR INFORMATION

Corresponding Author

*Seigo Shima: phone, ++49-(0) 6421-178-122; fax, ++49-(0) 6421-178-109; e-mail, shima@mpi-marburg.mpg.de. Ulrich Ermler: phone, ++49-(0)69-6303-1054; fax, ++49-(069)-6303-1002; e-mail, ulrich.ermler@biophys.mpg.de.

Funding

This work was supported by IMPRS (Structure and Function of Biological Membranes) the Japan Science and Technology Agency (JST), and the Max Planck Society.

Notes

The authors declare no competing financial interest.

■ ACKNOWLEDGMENTS

We thank Rudolf K. Thauer for discussion and for reading the manuscript, Hartmut Michel for continuous support, and the staff of PXII at the Swiss-Light-Source in Villigen (Switzerland) for help during data collection.

■ ABBREVIATIONS

H_4MPT, tetrahydromethanopterin; H_4F, tetrahydrofolate; Mch, methenyl-H_4MPT cyclohydrolase; aMch, Mch of *Archaeoglobus fulgidus*

■ REFERENCES

(1) Donnelly, M. I., Escalante-Semerena, J. C., Rinehart, K. L., Jr., and Wolfe, R. S. (1985) Methenyl-tetrahydromethanopterin cyclohydrolase in cell extracts of *Methanobacterium*. *Arch. Biochem. Biophys. 242*, 430−439.

(2) Breitung, J., and Thauer, R. K. (1990) Formylmethanofuran: tetrahydromethanopterin formyltransferase from *Methanosarcina barkeri*. Identification of N5-formyltetrahydromethanopterin as the product. *FEBS Lett. 275*, 226−230.

(3) Thauer, R. K. (1998) Biochemistry of methanogenesis: a tribute to Marjory Stephenson. 1998 Marjory Stephenson Prize Lecture. *Microbiology 144* (Pt 9), 2377−2406.

(4) Klein, A. R., Breitung, J., Linder, D., Stetter, K. O., and Thauer, R. K. (1993) N5,N10-methenyltetrahydromethanopterin cyclohydrolase from the extremely thermophilic sulfate reducing *Archaeoglobus fulgidus*: comparison of its properties with those of the cyclohydrolase from the extremely thermophilic *Methanopyrus kandleri*. *Arch. Microbiol. 159*, 213−219.

(5) Chistoserdova, L., Vorholt, J. A., Thauer, R. K., and Lidstrom, M. E. (1998) C1 transfer enzymes and coenzymes linking methylotrophic bacteria and methanogenic Archaea. *Science 281*, 99−102.

(6) Zellner, G., Stackerbrandt, E., Kneifel, H., Messner, P., Sleytr, U., Conway de Macario, E., Zabel, H. P., Stetter, K., and Winter, J. (1989) Isolation and characterization of a thermophilic, sulfate reducing archaebacterium, *Archaeoglobus fulgidus* strain Z. *Syst. Appl. Microbiol. 11*, 151−160.

(7) Hallam, S. J., Putnam, N., Preston, C. M., Detter, J. C., Rokhsar, D., Richardson, P. M., and DeLong, E. F. (2004) Reverse methanogenesis: testing the hypothesis with environmental genomics. *Science 305*, 1457−1462.

(8) DiMarco, A. A., Donnelly, M. I., and Wolfe, R. S. (1986) Purification and properties of the 5,10-methenyltetrahydromethanopterin cyclohydrolase from *Methanobacterium thermoautotrophicum*. *J. Bacteriol. 168*, 1372−1377.

(9) Vaupel, M., Dietz, H., Linder, D., and Thauer, R. K. (1996) Primary structure of cyclohydrolase (Mch) from *Methanobacterium thermoautotrophicum* (strain Marburg) and functional expression of the mch gene in *Escherichia coli*. *Eur. J. Biochem. 236*, 294−300.

(10) te Brommelstroet, B. W., Hensgens, C. M., Geerts, W. J., Keltjens, J. T., van der Drift, C., and Vogels, G. D. (1990) Purification and properties of 5,10-methenyltetrahydromethanopterin cyclohydrolase from *Methanosarcina barkeri*. *J. Bacteriol. 172*, 564−571.

(11) Breitung, J., Schmitz, R., Stetter, K., and Thauer, R. (1991) N5, N10-Methenyltetrahydromethanopterin cyclohydrolase from the extreme thermophile *Methanopyrus kandleri*: increase of catalytic efficiency (kcat/Km) and thermostability in the presence of salts. *Arch. Microbiol. 156*, 517−524.

(12) Pomper, B. K., Vorholt, J. A., Chistoserdova, L., Lidstrom, M. E., and Thauer, R. K. (1999) A methenyl tetrahydromethanopterin cyclohydrolase and a methenyl tetrahydrofolate cyclohydrolase in *Methylobacterium extorquens* AM1. *Eur. J. Biochem. 261*, 475−480.

(13) Vaupel, M., Vorholt, J. A., and Thauer, R. K. (1998) Overproduction and one-step purification of the N5,N10-methenyltetrahydromethanopterin cyclohydrolase (Mch) from the hyperthermophilic *Methanopyrus kandleri*. *Extremophiles 2*, 15−22.

(14) Grabarse, W., Vaupel, M., Vorholt, J. A., Shima, S., Thauer, R. K., Wittershagen, A., Bourenkov, G., Bartunik, H. D., and Ermler, U. (1999) The crystal structure of methenyltetrahydromethanopterin cyclohydrolase from the hyperthermophilic archaeon *Methanopyrus kandleri*. *Structure 7*, 1257−1268.

(15) Cohen, L., and Mackenzie, R. E. (1978) Methylenetetrahydrofolate dehydrogenase-methenyltetrahydrofolate cyclohydrolase-formyltetrahydrofolate synthetase from porcine liver. Interaction between the dehydrogenase and cyclohydrolase activities of the multifunctional enzyme. *Biochim. Biophys. Acta 522*, 311−317.

(16) Greenberg, D. M. (1963) [54] Synthesis and transformers of folic coenzymes II. Cyclohydrolase (5,10-methenyl to 10-formyl): 5,10-methenyltetrahydrofolic acid + H_2O → 10-formyltetrahydrofolic acid. *Methods Enzymol. 6*, 386−387.

(17) Allaire, M., Li, Y., MacKenzie, R. E., and Cygler, M. (1998) The 3-D structure of a folate-dependent dehydrogenase/cyclohydrolase bifunctional enzyme at 1.5 Å resolution. *Structure 6*, 173−182.

(18) Lee, W. H., Sung, M. W., Kim, J. H., Kim, Y. K., Han, A., and Hwang, K. Y. (2011) Crystal structure of bifunctional 5, 10-methylenetetrahydrofolate dehydrogenase/cyclohydrolase from *Thermoplasma acidophilum*. *Biochem. Biophys. Res. Commun. 406*, 459−463.

(19) Shen, B. W., Dyer, D. H., Huang, J. Y., D'Ari, L., Rabinowitz, J., and Stoddard, B. L. (1999) The crystal structure of a bacterial, bifunctional 5,10 methylene-tetrahydrofolate dehydrogenase/cyclohydrolase. *Protein Sci. 8*, 1342−1349.

(20) Schmidt, A., Wu, H., MacKenzie, R. E., Chen, V. J., Bewly, J. R., Ray, J. E., Toth, J. E., and Cygler, M. (2000) Structures of three inhibitor complexes provide insight into the reaction mechanism of the human methylenetetrahydrofolate dehydrogenase/cyclohydrolase. *Biochemistry 39*, 6325−6335.

(21) Sundararajan, S., and MacKenzie, R. E. (2002) Residues involved in the mechanism of the bifunctional methylenetetrahydrofolate dehydrogenase-cyclohydrolase: the roles of glutamine 100 and aspartate 125. *J. Biol. Chem. 277*, 18703−18709.

(22) Benkovic, S. J. (1978) On the mechanisms of folate cofactors. *Acc. Chem. Res. 11*, 314−320.

(23) Benkovic, S. J., Bullard, W., and Benkovic, P. (1972) Models for tetrahydrofolic acid. III. Hydrolytic interconversions of the tetrahydroquinoxaline analogs at the formate level of oxidation. *J. Am. Chem. Soc. 94*, 7542−7549.

(24) Robinson, D. R., and Jencks, W. P. (1967) Mechanism and catalysis of the hydrolysis of methenyltetrahydrofolic acid. *J. Am. Chem. Soc. 89*, 7098−7103.

(25) Robinson, D. R. (1970) Direct Observation of a Tetrahedral Intermediate during Amidine Hydrolysis. *J. Am. Chem. Soc. 92*, 3138−3146.

(26) Keltjens, J. T., Raemakers-Franken, P. C., Vogels, G. D. (1993) Methanopterin, its structural diversity and functional uniqueness in *Mikrobial Growth on C_1 compounds* (Murrel, J. C., Kelly, D. P., Eds.), pp 135−150, Intercept Ltd., Andover, U.K.

(27) Kallen, R. G., and Jencks, W. P. (1966) The dissociation constants of tetrahydrofolic acid. *J. Biol. Chem. 241*, 5845−5850.

(28) Maden, B. (2000) Tetrahydrofolate and tetrahydromethanopterin compared: functionally distinct carriers in C1 metabolism. *Biochem. J. 350*, 609−629.

(29) Gorris, L. G., Voet, A. C., and van der Drift, C. (1991) Structural characteristics of methanogenic cofactors in the non-methanogenic archaebacterium *Archaeoglobus fulgidus*. *Biofactors 3*, 29−35.

(30) White, R. H. (1988) Structural diversity among methanofurans from different methanogenic bacteria. *J. Bacteriol. 170*, 4594−4597.

(31) Shima, S., and Thauer, R. K. (2001) Tetrahydromethanopterin-specific enzymes from *Methanopyrus kandleri*. *Methods Enzymol 331*, 317−353.

(32) Lineweaver, H., and Burk, D. (1934) The determination of enzyme dissociation constants. *J. Am. Chem. Soc. 56*, 658−666.

(33) Kabsch, W. (2010) XDS. *Acta Crystallogr., D: Biol. Crystallogr. 66*, 125−132.

(34) McCoy, A. J., Grosse-Kunstleve, R. W., Adams, P. D., Winn, M. D., Storoni, L. C., and Read, R. J. (2007) Phaser crystallographic software. *J. Appl. Crystallogr. 40*, 658−674.

(35) Murshudov, G. N., Vagin, A. A., and Dodson, E. J. (1997) Refinement of macromolecular structures by the maximum-likelihood method. *Acta Crystallogr., D: Biol. Crystallogr. 53*, 240−255.

(36) Emsley, P., and Cowtan, K. (2004) Coot: model-building tools for molecular graphics. *Acta Crystallogr., D: Biol. Crystallogr. 60*, 2126−2132.

(37) Laskowski, R. A., MacArthur, M. W., Moss, D. S., and Thornton, J. M. (1993) PROCHECK: a program to check the stereochemical quality of protein structures. *J. Appl. Crystallogr. 26*, 283−291.
(38) Schrodinger, LLC (2010) *The PyMOL Molecular Graphics System, Version 1.3r1*.
(39) Holm, L., and Rosenström, P. (2010) Dali server: conservation mapping in 3D. *Nucleic Acids Res. 38*, W545−W549.
(40) Berman, H. M., Westbrook, J., Feng, Z., Gilliland, G., Bhat, T., Weissig, H., Shindyalov, I. N., and Bourne, P. E. (2000) The protein data bank. *Nucleic Acids Res. 28*, 235−242.
(41) Acharya, P., Goenrich, M., Hagemeier, C. H., Demmer, U., Vorholt, J. A., Thauer, R. K., and Ermler, U. (2005) How an Enzyme Binds the C1 Carrier Tetrahydromethanopterin. *J. Biol. Chem. 280*, 13712−13719.
(42) DiMarco, A. A., Bobik, T. A., and Wolfe, R. S. (1990) Unusual coenzymes of methanogenesis. *Annu. Rev. Biochem. 59*, 355−394.
(43) May, M., Bardos, T. J., Barger, F. L., Lansford, M., Ravel, J. M., Sutherland, G. L., and Shive, W. (1951) Synthetic and degradative investigations of the structure of folinic acid-SF. *J. Am. Chem. Soc. 73*, 3067−3075.
(44) Wolan, D. W., Cheong, C. G., Greasley, S. E., and Wilson, I. A. (2004) Structural insights into the human and avian IMP cyclohydrolase mechanism via crystal structures with the bound XMP inhibitor. *Biochemistry 43*, 1171−1183.
(45) Kang, Y. N., Tran, A., White, R. H., and Ealick, S. E. (2007) A novel function for the N-terminal nucleophile hydrolase fold demonstrated by the structure of an archaeal inosine monophosphate cyclohydrolase. *Biochemistry 46*, 5050−5062.
(46) Choi, K. H., Shi, J., Hopkins, C. E., Tolan, D. R., and Allen, K. N. (2001) Snapshots of catalysis: the structure of fructose-1,6-(bis)phosphate aldolase covalently bound to the substrate dihydroxyacetone phosphate. *Biochemistry 40*, 13868−13875.
(47) Sniegowski, J. A., Lappe, J. W., Patel, H. N., Huffman, H. A., and Wachter, R. M. (2005) Base catalysis of chromophore formation in Arg96 and Glu222 variants of green fluorescent protein. *J. Biol. Chem. 280*, 26248−26255.
(48) Rebelo, J., Auerbach, G., Bader, G., Bracher, A., Nar, H., Hosl, C., Schramek, N., Kaiser, J., Bacher, A., Huber, R., and Fischer, M. (2003) Biosynthesis of pteridines. Reaction mechanism of GTP cyclohydrolase I. *J. Mol. Biol. 326*, 503−516.
(49) Ren, J., Kotaka, M., Lockyer, M., Lamb, H. K., Hawkins, A. R., and Stammers, D. K. (2005) GTP cyclohydrolase II structure and mechanism. *J. Biol. Chem. 280*, 36912−36919.
(50) Morrison, S. D., Roberts, S. A., Zegeer, A. M., Montfort, W. R., and Bandarian, V. (2008) A new use for a familiar fold: the X-ray crystal structure of GTP-bound GTP cyclohydrolase III from *Methanocaldococcus jannaschii* reveals a two metal ion catalytic mechanism. *Biochemistry 47*, 230−242.